ISSN 1063-780X, Plasma Physics Reports, 2014, Vol. 40, No. 12, pp. 939–954. © Pleiades Publishing, Ltd., 2014.
Original Russian Text © V.V. Aleksandrov, V.A. Gasilov, E.V. Grabovski, A.N. Gritsuk, Ya.N. Laukhin, K.N. Mitrofanov, G.M. Oleinik, O.G. Ol'khovskaya, P.V. Sasorov, V.P. Smirnov, I.N. Frolov, A.P. Shevel'ko, 2014, published in Fizika Plazmy, 2014, Vol. 40, No. 12, pp. 1057–1073.

PLASMA DYNAMICS

Increase in the Energy Density of the Pinch Plasma in 3D Implosion of Quasi-Spherical Wire Arrays

V. V. Aleksandrov[a], V. A. Gasilov[b], E. V. Grabovski[a], A. N. Gritsuk[a], Ya. N. Laukhin[a], K. N. Mitrofanov[a], G. M. Oleinik[a], O. G. Ol'khovskaya[b], P. V. Sasorov[a], V. P. Smirnov[a], I. N. Frolov[a], and A. P. Shevel'ko[c]

[a] *Troitsk Institute for Innovation and Fusion Research, Troitsk, Moscow, 142190 Russia*
[b] *Keldysh Institute of Applied Mathematics, Russian Academy of Sciences, Miusskaya pl. 4, Moscow, 125047 Russia*
[c] *Lebedev Physical Institute, Russian Academy of Sciences, Leninskii pr. 53, Moscow, 119991 Russia*
e-mail: griar@triniti.ru, alexvv@triniti.ru

Received April 4, 2014

Abstract—Results are presented from experimental studies of the characteristics of the soft X-ray (SXR) source formed in the implosion of quasi-spherical arrays made of tungsten wires and metalized kapron fibers. The experiments were carried out at the Angara-5-1 facility at currents of up to 3 MA. Analysis of the spatial distribution of hard X-ray emission with photon energies above 20 keV in the pinch images taken during the implosion of quasi-spherical tungsten wire arrays (QTWAs) showed that a compact quasi-spherical plasma object symmetric with respect to the array axis formed in the central region of the array. Using a diffraction grazing incidence spectrograph, spectra of SXR emission with wavelengths of 20–400 Å from the central, axial, and peripheral regions of the emission source were measured with spatial resolutions along the array radius and height in the implosion of QTWAs. It is shown that the emission spectra of the SXR sources formed under the implosion of quasi-spherical and cylindrical tungsten wire arrays at currents of up to 3 MA have a maximum in the wavelength range of 50–150 Å. It is found that, during the implosion of a QTWA with a profiled linear mass, a redistribution of energy in the emission spectrum takes place, which indicates that, during 3D implosion, the energy of longitudinal motion of the array material additionally contributes to the radiation energy. It is also found that, at close masses of the arrays and close values of the current in the range of 2.4–3 MA, the average energy density in the emission source formed during the implosion of a quasi-spherical wire array is larger by a factor of 7 than in the source formed during the implosion of a cylindrical wire array. The experimental data were compared with results of 3D simulations of plasma dynamics and radiation generation during the implosion of quasi-spherical wire arrays with a profiled mass by using the MARPLE-3D radiative magnetohydrodynamic code, developed at the Keldysh Institute of Applied Mathematics, Russian Academy of Sciences.

DOI: 10.1134/S1063780X14110014

1. INTRODUCTION

Results of radiative magnetohydrodynamic (MHD) simulations [1] of the implosion of a quasi-spherical system consisting of a double-shell wire array and dynamic hohlraum in the fast Z-pinch mode [2, 3] demonstrated that the radiation intensity in the geometric center of such a system can be increased due to 3D concentration of the kinetic energy of plasma flows. 3D compression of the array material by the magnetic field during the implosion of quasi-spherical wire arrays (QWAs) was observed experimentally at the Angara-5-1 facility [4, 5].

Thus, 3D compression of plasma flows during QWA implosion allows one to more efficiently utilize the kinetic energy of the compressed substance for creating a soft X-ray (SXR) source as compared to 2D compression in cylindrical wire arrays (CWAs).

During QWA and CWA implosion, a region characterized by high values of the plasma density and its gradient forms in the central region of the pinch due to the concentration of plasma flows. Studies of the spatial distribution of the plasma density in such regions by laser probing and pulsed SXR radiography are hampered due to substantial refraction of laser radiation and strong absorption of SXR emission in dense plasma.

It is also difficult to record images of the pinch formed during the implosion of a wire array in its SXR self-radiation in the photon energy range of 0.1–0.6 keV, because, if the linear mass of the array is not matched to the amplitude and rise time of the discharge current, then a region containing plasma of the trailing array material forms at the pinch periphery. The trailing plasma affects the current distribution in

Table

Shot no.	Number and material of array wires/fibers	Layers of additional mass on the wires	Electrode type	Total array mass, μg
4944	30 W	–	plane	248
4961	40 W	–	plane	220
5017	16 W	Bi	plane	177
5071	30 W	Bi	plane	435
5094	40 kapron	In–Bi	conical	269
5096	40 kapron	In–Bi	conical	378
5101	30 W	Bi	conical	381

the pinch due to the shunting of a fraction of the discharge current and decreases the efficiency of plasma compression. Moreover, absorption of the pinch self-radiation in the trailing array material can distort the initial emission spectrum of the pinch. For this reason, when measuring the SXR spectra of the pinch, the initial linear mass of the arrays was chosen such that, for the experimental determined plasma production rate $\dot{m}_{\text{exp}}$, the material of the wire array at its initial radius was completely depleted by the instant corresponding to the maximum of the discharge current. The depletion of the wire material at the initial array radius was verified by the absence of the wire optical glow in the radial streak image of the array.

The spatial distribution of substance in the pinch was determined using pinch images taken in hard X-ray (HXR) photons (>20 keV). In [6, 7], generation of HXR emission during the implosion of different types of wire arrays was studied experimentally. It was found that HXR emission was usually generated several nanoseconds later than the peak of the SXR power. It was shown that the observed HXR pulses were related to bremsstrahlung caused by a fast electron beam [8, 9] interacting with tungsten ions entering into in the composition of the pinch plasma [6, 7]. Pinch images in photons with energies above 20 keV were obtained by applying specially designed HXR pinhole cameras [9].

In the present work, the parameters of pinch radiation generated during 3D implosion of wire arrays were studied using a spectrograph with a spatial resolution allowing one to record radiation from both the central part of the pinch and the trailing mass. To study the dynamics of array implosion in the radial and axial directions, optical streak images were used [5].

The aim of the present work was to study conditions for the formation of the SXR source in the center of a QWA, to compare the results of implosion for QWAs and CWAs, and to simulate the dynamics of 3D implosion and radiation generation for QWAs with masses profiled along the wire length by using the MARPLE-3D radiative MHD code, developed at the Keldysh Institute of Applied Mathematics, Russian Academy of Sciences.

2. EXPERIMENTAL LAYOUT

The implosion of different types of loads was studied experimentally at the Angara-5-1 eight-module electrophysical facility [4, 5]. The experiments were carried out in a vacuum chamber with a residual pressure of 10^{-5} Torr at discharge currents of 2–3.5 MA and current rise times of 90–100 ns.

Cylindrical and quasi-spherical arrays made of tungsten wires and of metalized kapron fibers with linear masses profiled along the array height were used as loads. A series of 52 experiments were carried out. The parameters of the arrays and the experimental results that will further be used in this paper are presented in the table.

The QWAs and quasi-spherical metalized fiber arrays (QMFAs) were formed by creating an electrostatic field between wires/metalized fibers of the original CWA and using an additional extending electrode installed in the discharge gap [4].

The linear array mass was profiled along the array length by depositing additional metal layers on different parts of the wires/fibers by the method of thermal evaporation of metals in vacuum in the VUP-4 vacuum setup [5].

Layers of metals with different atomic numbers (aluminum, indium, and bismuth) were deposited. The quality of metal deposition was verified using test samples by measuring the wire diameter and deposition homogeneity with the help of a scanning electron microscope and an X-ray spectrograph analyzer, respectively [5].

In order to increase the implosion efficiency and achieve the maximum power of SXR emission, the radii and linear masses of CWAs for a given time profile of the discharge current $I(t)$ and a given linear mass m of the compressed material were chosen by solving the Newton equation

$$\frac{m}{2\pi r}\ddot{r} = -\frac{B^2}{2\mu} = -\frac{\mu I(t)^2}{8\pi^2 r^2}, \quad (1)$$

with the additional condition that, for this linear mass m, the velocity of the array material should reach its maximum value near the peak of the pinch current.

As was noted above, when manufacturing QWAs and QMFAs, additional metal layers were deposited on the wires or fibers along their height. The metal was deposited on a QWA (or QMFA) with a radius R_{QWA} in the equatorial plane in such a way that the profiled linear mass satisfied the condition

$$mR_{QWA}^2 \sin^2\theta = \text{const}, \quad (2)$$

where θ is the poloidal angle [1].

The experiments were carried with QWAs and QMFAs with a total mass of 150–450 μg and height of 15 mm. The arrays occupied a part of a quasi-spherical surface with a radius $R_{QWA} = 9.6$ mm.

A QWA with a radius R_{QWA}, height of 4 mm, conical anode, and conical cathode is shown schematically in Fig. 1.

Under the action of the electrostatic field applied to the wires of the original CWA (item *1*) and the additional extending electrode (item *2*), the outer boundary of the array takes an axisymmetric quasi-spherical shape with truncated poles near the anode and cathode.

The parameters of the array implosion were measured using the diagnostic complex of the Angara-5-1 facility [5, 10]. The waveforms of the discharge current and voltage, as well as of the electric power supplied from the eight-module current generator of the Angara-5-1 facility to the load (array), were measured using eight calibrated detectors of the current time derivative mounted in front of each module and an inductive voltage divider. The waveforms of the discharge current and voltage were used to calculate the time dependences of the pinch inductance and the effective current radius of the discharge. The power and spatial anisotropy of the pinch SXR emission were measured using two identical sets of four vacuum X-ray detectors (XRDs) on the basis of open vacuum photodiodes equipped with different X-ray filters. These sets of XRDs were used to measure the SXR powers emitted perpendicular to the array axis (in the radial direction) and at an angle of 7° to the array axis (nearly in the axial direction).

To study how the implosion parameters depend on the type and parameters of the load, we used 2D images obtained with an X-ray pinhole camera in two photon energy ranges, above 100 eV (behind a Mylar film with a thickness of 2 μm) and above 600 eV (behind an aluminum foil with a thickness of 3 μm), and recorded on VRP high-resolution photoplates [9]. The transmission curves of X-ray filters as functions of the photon energy were obtained using tables from [11].

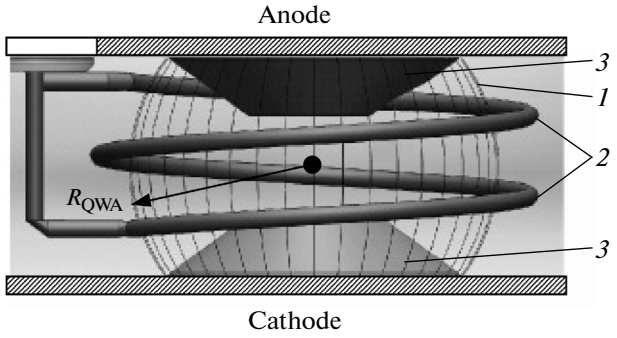

Fig. 1. Design of a QWA with a radius of $R_{QWA} = 9.6$ mm and conical insertions of height 4 mm: (*1*) QWA-wires, (*2*) additional extending electrode, and (*3*) conical insertions on the anode and cathode sides. The distance between the conical anode and conical cathode is 7 mm, the pitch of the additional helical electrode is 5 mm, and the diameter of the additional electrode is 1.3 mm.

X-ray images of a pinch taken in the photon energy range above 20 keV were also recorded using pinhole cameras. The design of the HXR pinhole camera provided high screening of the HXR sensor (an RF-3 X-ray film) from scattered HXR photons with energies of up to a few hundred keV, generated at the electrodes. Photons with such high energies are generated in vacuum transmission lines (VTLs) due to the deceleration of electrons of the leakage current onto the VTL electrodes during the establishment of magnetic self-insulation. The intense HXR background thus produced at the location of the X-ray film was suppressed by two orders of magnitude by means of a lead screen.

SXR spectra of the Z-pinch plasma in the wavelength range of 20–400 Å were recorded using a diffraction grazing incidence spectrometer (GIS) with a 40-μm-wide entrance slit and a 20 × 30 mm concave diffraction grating (the curvature radius $R = 1$ m, the grazing angle of 4°, and W/Re coating) [12]. The spectrograph was mounted at 150 cm from the facility axis. The spectra were recorded on the absolutely calibrated UF-4 emulsionless film. The dynamic range of the film was about two orders of magnitude, provided that the technology of its development after the exposure are satisfied [13, 14]. The distribution of the SXR spectral intensity was obtained with allowance for the spectral sensitivity of the UF-4 film and the reflection coefficient of SXR emission from the diffraction grating.

To obtain a spatially resolved spectrum, an additional (spatial) slit was installed in front of the GIS, which made it possible to produce a 1D pinch image at the entrance slit of the spectrometer.

The optical scheme of the GIS is shown in Fig. 2.

The radiation incident through the entrance slit on the diffraction grating is decomposed into the spectrum and focused on the Rowland circle. In the off-Rowland scheme used in the spectrograph, the spectrum is recorded in a plane perpendicular to diffracted

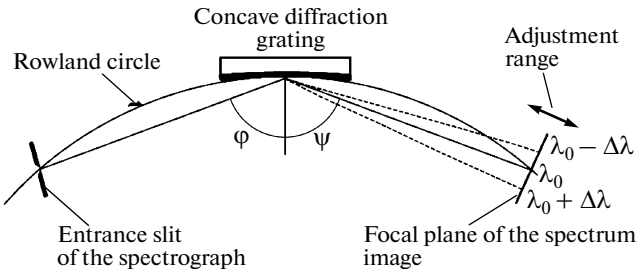

Fig. 2. Optical scheme of a diffraction GIS with an off-Rowland configuration of spectrum recording. Here, ϕ is the angle of incidence of X radiation on the concave diffraction grating, ψ is the diffraction angle of X radiation with a wavelength λ_0, and $\Delta\lambda$ is the spectral range of spectrum recording.

rays (Fig. 2). In this method, only for one (central) wavelength λ_0 corresponding to the intersection of the recording plane with the Rowland circle is focused precisely. Due to the small aperture of the spectrograph, the spectrum can be recorded in a relatively wide spectral range of $\lambda_0 \pm \Delta\lambda$.

To obtain an image of the spectrum of an SXR emission source with a spatial resolution along the pinch height, the spatial slit was oriented perpendicular to the entrance slit of the GIS. For such a mutual orientation of the slits, a 1D image of the pinch spectrum with a spatial resolution along the height between the anode and cathode is produced in the film plane after reflection from the diffraction grating. This image contains information on the distributions of the SXR spectral intensity at different distances between anode and cathode.

To record the SXR spectrum of the pinch with a spatial resolution in the direction perpendicular to the symmetry axis (along the radius), the spatial slit of the GIS is oriented in the direction parallel to the symmetry axis of the source. This means that the GIS with the entrance slit and grating should be rotated by an angle of 90°, i.e., the spatial slit should be perpendicular to the entrance slit. For such a mutual orientation of the slits, an image of the pinch spectrum with a spatial resolution along the source radius is produced in the film plane.

The scheme of recording X-ray spectra of the Z-pinch by a GIS with spatial resolutions in the radial and axial directions is shown in Fig. 3. In this scheme, spatial slit S_1 is used to obtain images of the spectra with spatial resolutions along the array radius and height. The slit is installed in front of the GIS as is shown in Fig. 3.

Entrance slit S_2 of the GIS was located at a distance of 150 cm from the pinch axis. The used optical scheme of producing a 1D pinch image allowed one to record the radiation spectrum in the range of 20–400 Å with a maximum spectral resolution of $\lambda/\Delta\lambda = 10^2$. The magnification of the optical system provided a spatial resolution of 1 mm on the object for photons with energies of 30 eV and 240 μm for photons with energies of about 500 eV.

To illustrate spatial resolution over the radius, Fig. 4 schematically shows an image of a pinch in the shape of a sphere. Two spherical layers are located at distances of R_1 and R_2 from the array axis (items *2* and *3*, respectively). The radiation of these layers forms 1D spectral images situated at distances of R_1M and R_2M from the central axis, respectively (here, M is the magnification of the optical scheme for producing a 1D pinch image).

The lead-screen protection of the GIS from scattered HXR emission decreased the film exposure by the hard spectral component to the original optical density of an unexposed film. The recording direction was adjusted to within 10^{-3} rad (1 mm on the object) by using an auxiliary laser.

The developed optical systems for recording 1D SXR images with spatial resolutions along the radius and height were used to determine the compactness of plasma compression and measure the dimensions of radiation sources in photons with different wavelengths. Depending on the mutual orientation of the spatial and entrance slits, the optical system allowed one to obtain information on the distribution of energy over the pinch radiation spectrum with a radial or an axial spatial resolution [14].

The dynamics of array implosion in the radial and axial directions was studied using an SFER-2 optical streak cameras [10].

An X-ray frame image tube with a sectioned microchannel plate and X-ray filters of different hardness was used to record 2D frame X-ray images of imploding arrays in photons of different hardness with a time exposure of 1.5 ns [14].

3. EXPERIMENTAL RESULTS

Experiments on the implosion of QWAs and QMFAs showed that conical electrode insertions and profiling of the array mass according to formula (2) lead to more symmetric density distributions of tungsten and bismuth ions in the array center and a decrease in the dimensions of the pinch images taken in the HXR and SXR emission.

Figure 5 shows HXR pinch images obtained in three shots with different types of quasi-spherical tungsten wire arrays (QTWAs) and different shapes of the electrodes: an array made of 30 tungsten wires without deposition of an additional mass (shot no. 4944; plane electrodes; the total array mass is 180 μg); an array made of 16 tungsten wires with deposition of additional metal layers near the plane anode and cathode (shot no. 5017; electrodes; the total array mass is 180 μg), and an array made of 30 tungsten wires

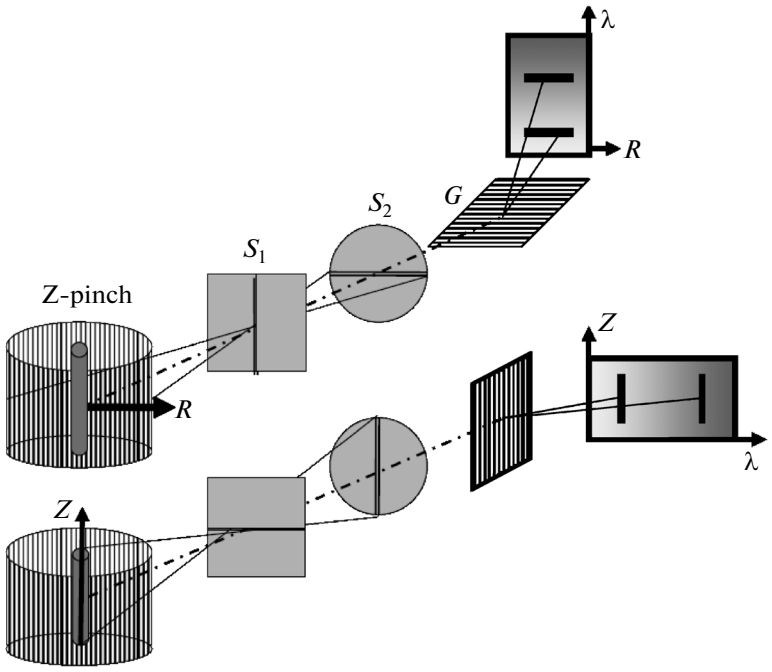

Fig. 3. Scheme of recording X-ray spectra of a Z-pinch by a GIS with spatial resolutions in the radial and axial directions. Here, Z is the axial observation direction, R is the radial observation direction, $R(\lambda)$ is the spectrum image with a radial resolution, $Z(\lambda)$ is the spectrum image with an axial resolution, S_1 is the spatial slit, and S_2 is the entrance slit.

with deposition of additional metal layers near the steel conical anode and cathode (shot no. 5101; the total array mass is 380 μg).

These images are formed due to the generation of fast electron beams arising in the course of implosion in the cathode region of the discharge. Propagation from the cathode toward the anode, fast electrons with energies of a few hundred keV interact with tungsten ions, which leads to the generation of HXR photons. The size of the pinch image taken in HXR photons allows one to estimate the characteristic pinch dimensions and the spatial distribution of the density of tungsten ions in the pinch [9].

Figure 5d shows the blackening profiles in images 5a–5c along a line parallel to the electrode planes and passing through the array center. Oscillations in the blackening profiles are associated with the finite dimensions of emulsion grains of the RF-3 high-contrast X-ray film. It is seen that, in the case of plane electrodes, mass profiling leads to a decrease in the diameter of the HXR source from 4.4 to 3.9 mm. In this case, the emission source formed in the central part of the pinch is more symmetric with respect to the axis. The use of conical electrodes and a profiled array mass (Fig. 5c) results in a decrease in the diameter of the HXR source to 3.3 mm and improves its spatial symmetry.

Similar qualitative conclusions follows from the analysis of time-integrated pinch images (Fig. 6) taken with a pinhole camera in the SXR self-emission with photon energies of >120 eV in the same shots as in Fig. 5.

It follows from Figs. 6a–6c that the intensity of the radiation source formed in the center of the imploding

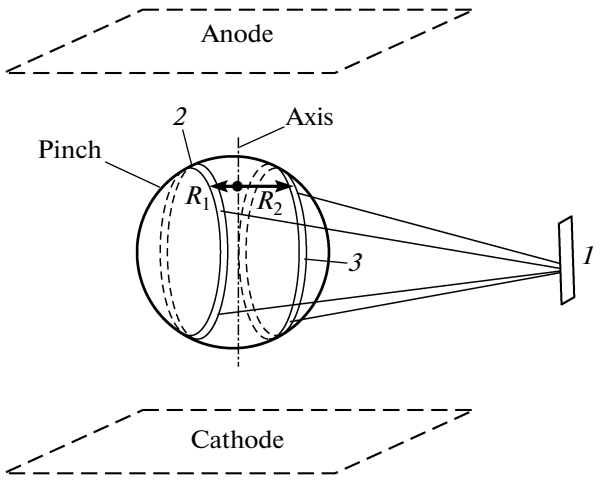

Fig. 4. Scheme of recording SXR spectra from pinch regions located at different distances from the pinch axis: (*1*) spatial slit and (*2, 3*) pinch regions that are located at distances R_1 and R_2 from the axis and over which the radiation intensity of the source is averaged.

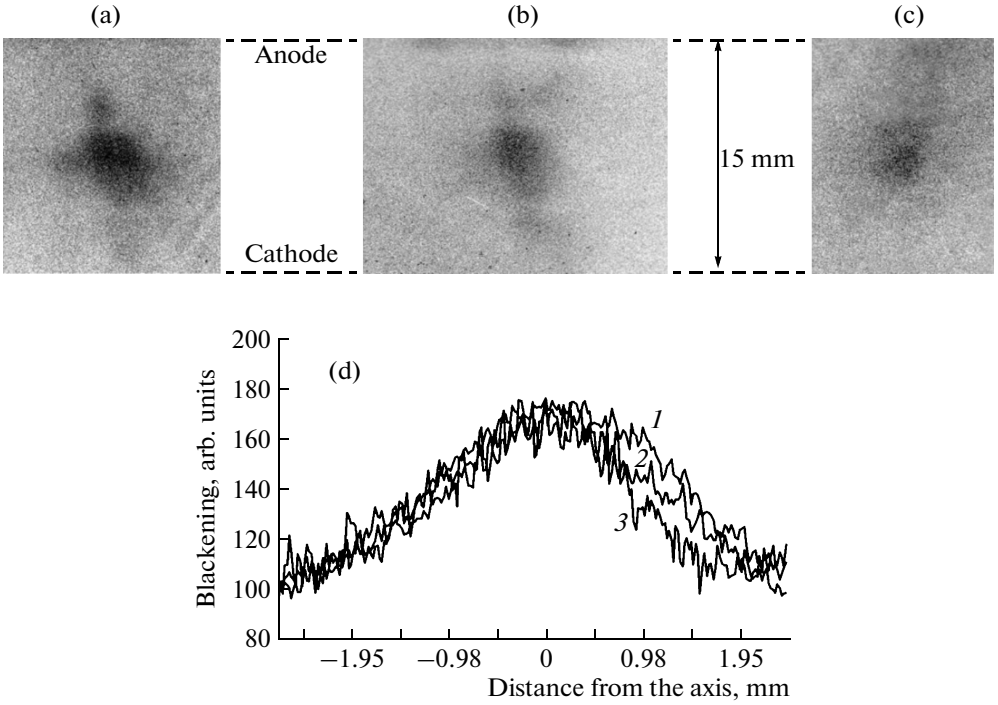

Fig. 5. (a–c) Time-integrated images (taken in HXR photons with energies above 20 keV) of the pinches formed in three shots with different types of QTWAs: (a) shot no. 4944 (30 W wires with a total mass of 165 μg; no additional deposition; the diameter of the central region of the array is 4.4 mm; plane electrodes), (b) shot no. 5017 (16 W-wires with a total mass of 177 μg; Bi deposition; the diameter of the central region of the array is 3.9 mm; plane electrodes), and (c) shot no. 5101 (30 W wires with a total mass of 380 μg; Bi deposition; the diameter of the central region of the array is 3.3 mm; conical electrodes). (d) Profile of the blackening in images (a), (b), and (c) along a line passing through the array center parallel to the electrode planes: (*1*) shot no. 4944, (*2*) shot no. 5017, and (*3*) shot no. 5101.

QTWA between the shadows of the wires of the extending electrode depends on the array type. Comparison of the QTWA images in Figs. 6a and 6b shows that the intensity of plasma radiation from the electrode regions decreases when using wires with a profiled mass. The decrease in the intensity in these regions, in turn, indicates that the profiling of the QTWA mass improves the compression of the wire material in the center of the arrays with plane electrodes.

Figure 6d shows the blackening profiles in images 6a–6c along a line parallel to the electrode plane and passing through the array center. The arrows show the full widths at half-maximum (FWHMs) of the emission sources: 4.9 mm in shot no. 4944, 3.2 mm in shot no. 5017, and 3.0 mm in shot no. 5101.

To study how the spatial distribution of the linear mass of a quasi-spherical array along its height affects the compression of the array material, we carried out experiments with QWAs and QMFAs. The profiling of the spatial distribution of the linear mass along the wires or fibers near the electrodes was performed by depositing additional layers of indium and bismuth by thermal sputtering in vacuum [5].

The results of measurements of the spatiotemporal parameters of the radiation source formed during QMFA implosion are presented in Fig. 7.

Figures 7a–7c show typical time-integrated pinch images taken in three photon energy ranges in the implosion of a QMFA with conical electrodes. The positions of the anode and cathode and the initial position of the array are shown by the dashed lines.

It is seen from Figs. 7a–7c that a quasi-spherical radiating plasma object forms in the center of the discharge gap. The formation of a compact axisymmetric radiation source between the anode and cathode indicates 3D compression of the array material during QMFA implosion.

The dynamics of array implosion was studied using two SFER-2 streak cameras. To record the time evolution of 1D images taken in the pinch self-radiation along the array radius and height, the slits of these cameras were oriented perpendicular and parallel to the array axis, respectively. The corresponding streak images of the pinch are called radial and axial streak images, respectively. Figures 7d and 7e show typical radial and axial steak images of an imploding QMFA and the synchronized waveforms of the power of SXR emission with photon energies above 120 eV (shot

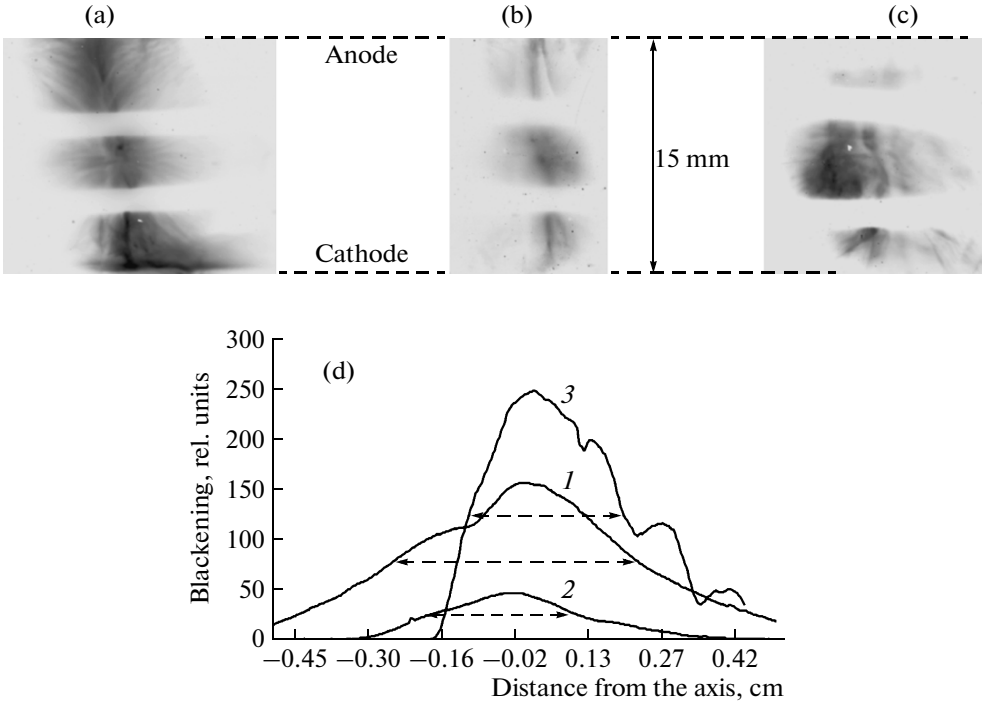

Fig. 6. (a–c) Time-integrated images (taken in SXR self-radiation with photon energies above 120 eV) of the pinches formed in three shots with different types of QTWAs with Bi-deposition: (a) shot no. 4944 (30 W wires with a total mass of 165 μg; no additional deposition; the diameter of the central region of the array is 4.9 mm; plane electrodes), (b) shot no. 5017 (16 W wires with a total mass of 177 μg; Bi deposition; the diameter of the central region of the array is 3.2 mm; plane electrodes), and (c) shot no. 5101 (30 W wires with a total mass of 380 μg; Bi deposition; the diameter of the central region of the array is 3.0 mm; conical electrodes). (d) Profiles of the blackening in images (a), (b), and (c) along a line passing through the array center parallel to the electrode planes: (*1*) shot no. 4944, (*2*) shot no. 5017, and (*3*) shot no. 5101.

no. 5094). In Fig. 7e, one can see the shadows of the extending electrostatic electrode.

In the radial streak image of the pinch (Fig. 7d), one can see weak emission from the equatorial part of the array compressed onto the center and an emission burst at the instant corresponding to the maximum of the SXR power. The SXR power reaches its maximum value when the plasma produced from all parts of the array reach the array center, after which the pinch plasma expands. In the axial streak image (Fig. 7e), emission from the center of the array appears only at the instant corresponding to the maximum of the SXR power.

Figure 8 shows waveforms of the discharge current and SXR power and three typical frame X-ray images taken at the same instant during QMFA implosion (4.6 ns before the peak of the SXR power) without a filter and behind a 6-μm-thick Al foil and 162-μg/cm^2 Mylar film (shot no. 5096).

Frame images of the imploding QMFA shown in Fig. 8 were taken in X rays of different hardness with a time exposure of 1.5 ns by using three pinhole cameras and an X-ray image tube.

Note that, at the instant corresponding to the maximum of the SXR power, the brightest region in typical frame X-ray images is located in the center of the load (Fig. 8b).

Thus, time-integrated and frame X-ray images, as well as optical streak images, taken during the implosion of QTWAs and QMFAs clearly indicate 3D compression of the array material.

The dimension of the SXR source is defined as the FWHM of the blackening profile in the time-integrated image of the source. The average size of the source is defined as the mean value of its dimensions along and across the array axis. In a series of experiments with QTWAs with Bi deposition, the average size of the source obtained using a pinhole camera behind a Mylar film (>120 eV) was 3.5 ± 0.7 mm, while that obtained in HXR emission (>20 keV) was 3.1 ± 0.3 mm. The average size of the source with photon energies above 120 eV that formed during the implosion of a QMFA with Bi–In deposition was 3.1 ± 0.8 mm. The above errors are determined by the statistical spread in the measurement results in a series of experiments performed at currents of 2–3.5 MA and current rise times of 90–100 ns.

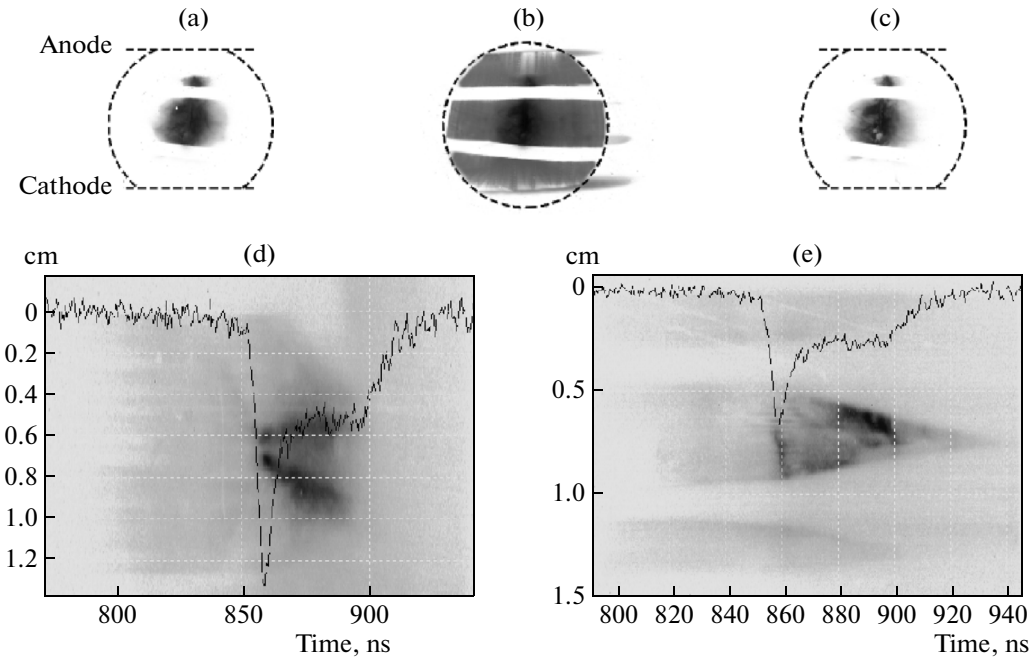

Fig. 7. (a–c) Images of the emission source formed during the implosion of a quasi-spherical array (shot no. 5094) made of 40 25-μm-diameter metalized kapron fibers with a total mass of 270 μg, profiled In–Bi deposition, and conical electrodes (the distance between the anode and cathode is 15 mm), taken with and without filters: (a) with a 316-μg/cm^2 Mylar film (>120 eV), (b) without a filter, and (c) with a 3-μm-thick Al foil (>600 eV); (d) radial and (e) axial optical streak images of the imploding array synchronized with the SXR pulse with photon energies above 120 eV.

Thus, in the Angara-5-1 experiments on the implosion of QTWAs and QMFAs with profiled linear masses and conical steel electrodes carried out at currents of 2–3.5 MA and current rise times of 90–100 ns, 3D compression of the array material and the formation of a compact intense quasi-spherical SXR source on the array axis were achieved.

The absence of wide wings in the distribution of the SXR pinch intensity and high energy concentration in the pinch center are important characteristics of compact 3D plasma compression during QWA implosion. The spatial characteristics of the emissivity of the compressed pinch plasma were studied by measuring the SXR emission spectrum with spatial resolutions across and along the array axis. For this purpose, we used a time-integrated GIS operating in the wavelength range of 20–400 Å with spatial resolutions along the array radius and height.

SXR emission spectra recorded with radial and axial resolutions in the implosion of a QTWA are shown in Fig. 9.

Figures 9a (shot no. 5071) and 9b (shot no. 4961) show SXR emission spectra with radial and axial resolutions, respectively, recorded during QTWA implosion. Two white bands in Fig. 9b are the shadows of the extending electrodes. The horizontal lines in Fig. 9a correspond to radii of 0, 2.2, and 3.8 mm. The distributions of the spectral intensity measured along these lines are shown in Fig. 9c.

The distributions of the spectral intensity measured at different heights above the cathode (along lines *1*, *2*, and *3* in Fig. 9b) are shown in Fig. 9d.

A specific feature of the dependence of the SXR spectral intensity on the photon energy in Fig. 9d is that the formation of a peak of the SXR intensity is observed in the emission spectrum of the central part of the array (curve *1*) in the photon energy range of 100–150 eV. Note that this maximum of the intensity is the most strongly pronounced for arrays with a spatially profiled linear mass.

Figure 10 compares the radiation spectra of CWA and QWA pinches obtained at close amplitudes of the discharge current and close values of the total array mass. Curves *1*, *2*, and *3* correspond to a QTWA (shot no. 5074), QMFA (shot no. 5096), and cylindrical tungsten wire array (CTWA) (shot no. 5091), respectively. It is seen from these spectra that, in contrast to quasi-spherical arrays (curves *1*, *2*), there is no intensity peak in the spectral range of 100–150 eV in the implosion of the cylindrical array (curve *3*). Such a peak appears due to the energy redistribution in the spectra of quasi-spherical arrays toward an increase in the number of photons in this spectral range, which indicates that 3D concentration of the energy of longitudinal motion of the array material during the implosion of quasi-spherical arrays additionally contributes to the total radiation energy.

It follows from the SXR spectra recorded with a radial resolution in QTWA implosion (Fig. 9c) that, at a distance of 2–3 mm from the axis, the spectral intensity in the wavelength range of 70–100 Å decreases 20–30 times as compared to that on the pinch axis.

Figure 11 shows the spectra of SXR emission recorded in CTWA implosion from regions located at different distances from the pinch axis. It should be noted that, for such loads, the maximum spectral intensity at a distance of 2–3 mm from the axis is only two to three times lower than that on the pinch axis (Fig. 11b).

The SXR spectra recorded with a radial resolution in QTWA (Fig. 9a) and CTWA (Fig. 11a) implosion allow one to determine the radii of the emitting pinch regions as functions of the radiation wavelength. It should be noted that the radii of the SXR sources obtained from the above spectral measurements coincide to within 10% with the radii of the sources in 2D X-ray pinhole images recorded behind a 316-μg/cm^2 Mylar film (Figs. 11a, 12a and [16]).

Thus, the radial distribution of the intensity of the X-ray source in the case of a QTWA decreases more rapidly from the center toward the periphery as compared to that in a CTWA (Figs. 9c, 11b). Comparison of the pinch radii obtained from the radially resolved SXR emission spectra recorded in the implosion of a QTWA and CTWA with close values of the total array mass show that the typical size of the emission source is somewhat smaller (by nearly 30%) for the QTWA. This means that the QTWA material in the emission source is compressed more efficiently as compared to that in the CTWA, namely, it is compressed to a smaller radius and the image of the QTWA emission source (Fig. 12b) looks more compact than in the case of a CTWA due to the absence of wings in the distribution of the pinch intensity (Fig. 12a).

It is seen from the SXR spectra shown in Fig. 11b that the shape of the spectrum of the trailing (peripheral) mass of the array (curve *3*) differs appreciably from that of the central pinch region (curve *1*). Curve *1* has typical features of a blackbody spectrum. At the same time, three spectral regions can be distinguished in the radiation of the trailing mass (curve *3*): 120–250, 80–120, and 45–70 Å. There regions are close to the calculated bands in the instantaneous emission spectra of a tungsten Z-pinch [15]; for the first time, they were observed experimentally in [16]. These bands in the spectrum of the trailing mass are related to the reemission of radiation from the central part of the pinch.

Figures 12a and 12b show time-integrated 2D SXR images of the pinch taken in photons with energies above 120 eV (behind a 316-μg/cm^2 Mylar film) in the implosion of a CTWA (shot no. 5091) and QMFA (shot no. 5094) at a current amplitude of 2.5 MA.

Note that, in the case of CTWA implosion, the diameter of the emitting region determined from the radially resolved spectra presented in Fig. 11a coincides with that determined from the image shown in Fig. 12a and is equal to $d_{CWA} = 5$ mm. For the array height $H = 15$ mm, the volume of the compressed plasma is $V = \pi d^2 H/4 = 0.29$ cm^3. The typical SXR energy emitted during the implosion of a 20-mm-diameter CWA made of 40 tungsten wires with a total linear mass of 220 μg/cm at a current of 2.5 MA is $E_{CWA} = 30$ kJ. Therefore, the SXR energy per unit volume of the X-ray source is 30 kJ/0.29 cm^3 = 103 kJ/cm^3.

In the case of a QMFA, the diameter of the emitting region in the image shown Fig. 12b is $D_{QMFA} =$ 3 mm and the volume of the compressed plasma is

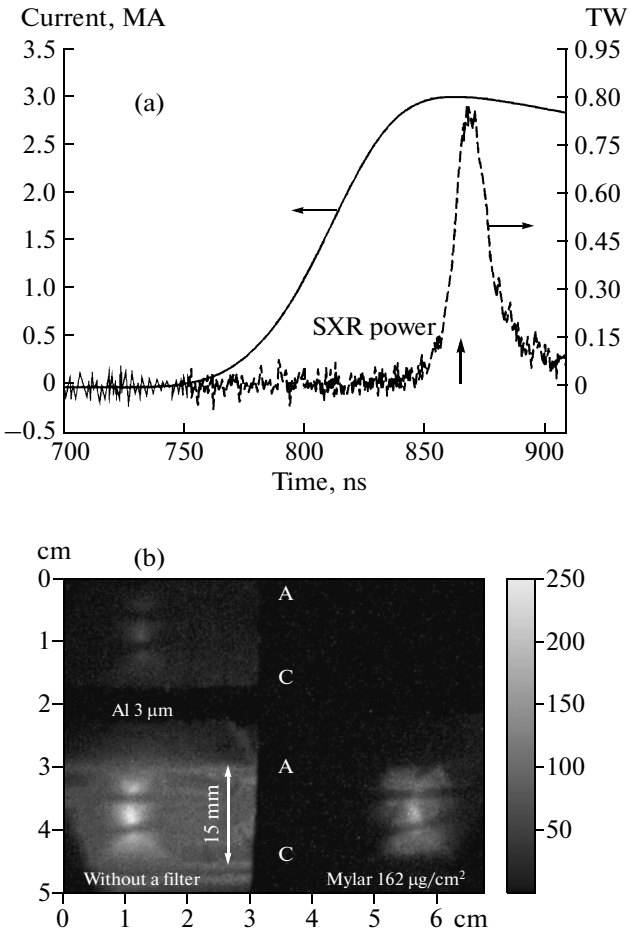

Fig. 8. (a) Waveforms of the discharge current and SXR power and (b) three frame images of the pinch taken in X rays of different hardness 4.6 ns before the peak of the SXR pulse with an exposure of 1.5 ns with and without filters: without a filter, with a 6-μm-thick Al foil, and with a 162-μg/cm^2 Mylar film (shot no. 5096; quasi-spherical array made of 40 25-μm-diameter metalized kapron fibers with a total mass of 380 μg, profiled In–Bi deposition, and conical electrodes; the distance between the anode and cathode is 15 mm). The vertical arrow in panel (a) shows the instant at which the frame images were taken.

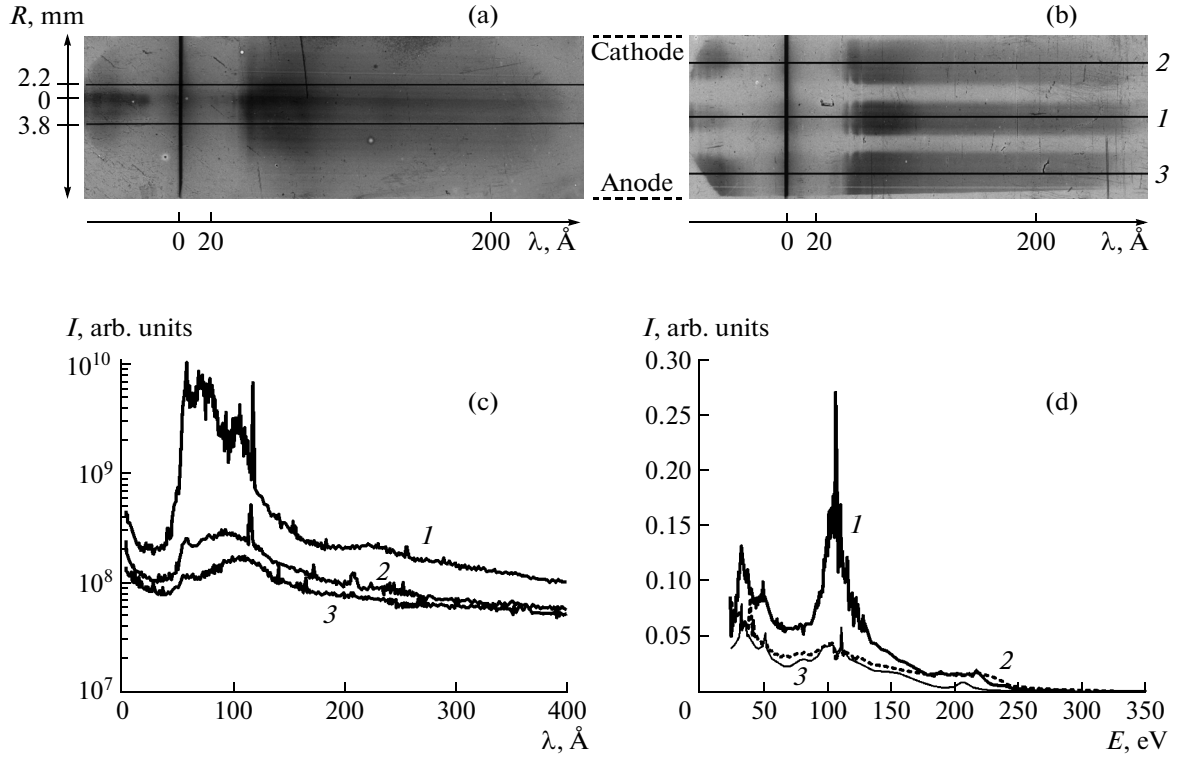

Fig. 9. SXR spectra recorded with (a) radial and (b) axial resolutions in the implosion of a QTWA and (c, d) emission spectra measured in the directions shown by the horizontal lines in panels (a) and (b), respectively: (a, c) shot no. 5071 (QTWA with a total mass of 435 μg) and (b, d) shot no. 4961 (QTWA with a total mass of 440 μg; the distance between the anode and cathode is 15 mm). Panel (c) show the spectral intensity vs. wavelength at different distances from the array axis: (*1*) on the axis, (*2*) at 2.2 mm from the axis, and (*3*) at 3.8 mm from the axis. Panel (d) shows the spectral intensity vs. photon energy at different heights above the cathode: (*1*) in the central part of the array between the extending electrodes, (*2*) between the cathode and the extending electrode, and (*3*) between the anode and the extending electrode.

$V_{\text{sphere}} = \pi d^3/6 = 3.14 \times 0.3^3/6 = 0.014$ cm^3. The SXR energy emitted in a shot with a current of 2.5 MA is $E_{\text{QMFA}} = 11$ kJ; accordingly, in this case, the SXR energy per unit volume of the X-ray source is 11 kJ/0.014 cm^3 = 785 kJ/cm^3.

Thus, during the implosion of QMFAs and CWAs with nearly the same total masses at a discharge current of 2.5 MA, the average SXR energy density in the volume of the source formed during QMFA implosion is a factor of 7.5 higher than that in the case of CTWA implosion. Such a ratio of the average densities of the radiation energy during the implosion of QMFAs and CWAs does not contradict the estimate obtained in [1].

4. 3D SIMULATION OF Z-PINCH COMPRESSION DURING THE IMPLOSION OF QUASI-SPHERICAL WIRE ARRAYS

Quasi-spherical compression of wire arrays was simulated using the 3D MARPLE-3D radiative MHD code, developed at the Keldysh Institute of Applied Mathematics, Russian Academy of Sciences [17, 18]. In the radiative MHD model, the magnetized plasma flow is described using a set of one-fluid MHD equations in Cartesian coordinates with allowance for anisotropy of dissipative processes, the energy balance is described in a two-temperature model that takes into account electron–ion energy exchange, and the radiative energy transfer is described in terms of a multigroup diffusion model. In these simulations, 36 spectral groups were used. The equations of state and optical properties of substances were calculated using the TERMOS software [19].

The simulations were aimed at studying the influence of the array geometry and the initial distribution of the array mass on the implosion process. In the numerical experiments, the implosions of different types of wire arrays with a profiled linear mass and plane and conical electrodes were compared. The simulations adequately reproduced the geometry of actual arrays. The electrodes were assumed to be perfectly conducting. The process of electrode erosion under the action of the discharge current pulse was disregarded, because the experimental conditions were chosen in such a way that the erosion mass flow from the electrodes insignificantly affected plasma compression in the center of the array. As a result of the numerical simulations, the distributions of the plasma

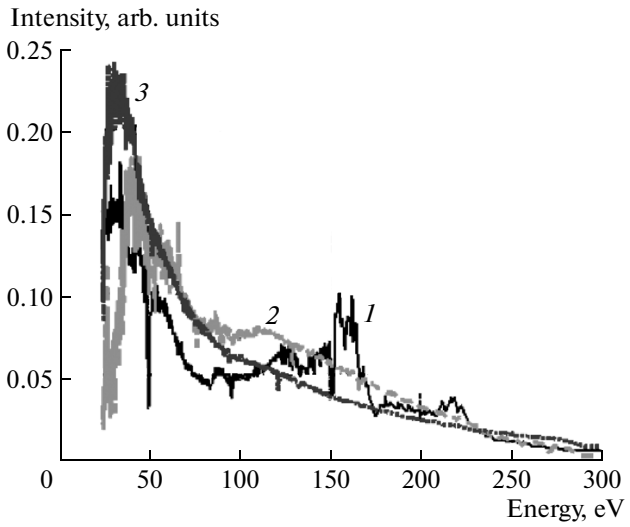

Fig. 10. Emission spectra of CWA and QWA pinches at close amplitudes of the discharge current and close values of the total array mass: (*1*) shot no. 5074 (QTWA), (*2*) shot no. 5096 (QMFA), and (*3*) shot no. 5091 (CTWA).

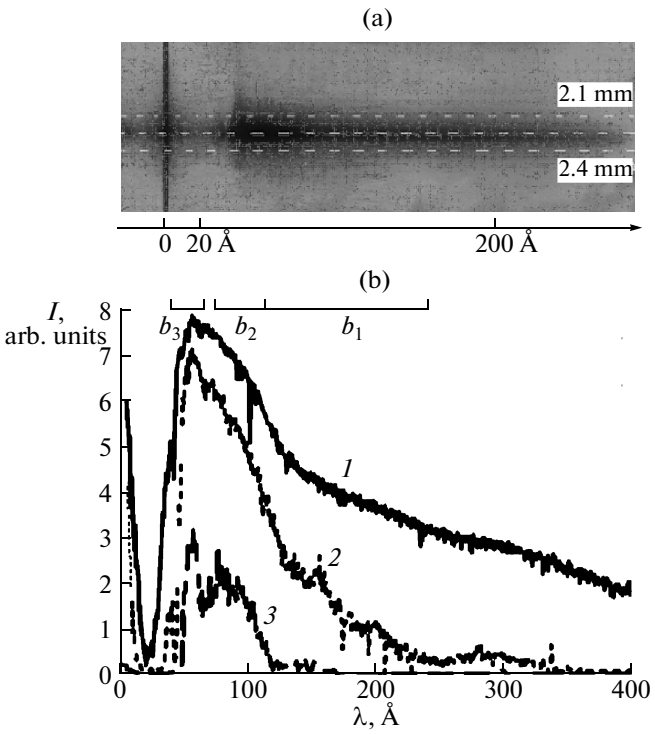

Fig. 11. (a) Typical emission spectrum recorded with a radial resolution in the center of the pinch formed during the implosion of a 20-mm-diameter cylindrical array made of 40 6-μm-diameter tungsten wires with a total linear mass of 220 μg/cm (shot no. 5091) and (b) spectral intensity vs. wavelength at different distances from the array axis: (*1*) at the axis, (*2*) at a radius of 2.1 mm, and (*3*) at a radius of 2.4 mm. The horizontal dashed lines in panel (a) show the directions in which the spectra shown in panel (b) were measured. The segments b_1, b_2, and b_3 in panel (b) denote the calculated spectral bands of tungsten radiation in the wavelength ranges of 120–250, 80–120, and 45–70 Å, respectively.

density and temperature in the emission source and the radiation power emitted in the course of pinch compression were determined.

Figure 13 shows a scheme of a quasi-spherical wire array with profiled electrodes used in the numerical experiments. The wire array was assumed to consist of 40 6-μm-diameter tungsten wires with a profiled linear mass achieved by depositing additional tungsten layers near the electrodes. The total array mass was 266 μg. The additional mass was distributed uniformly over 4.54-mm-long segments of the wires adjacent to the anode and cathode, the wire mass per unit length in these segments being 188 μg/cm. The wire mass per unit length in the 8.134-mm-long middle segments without additional deposition was 117 μg/cm.

The calculations were performed in a 45° cylindrical sector with periodic boundary conditions at $\varphi = 0$ and $\varphi = \pi/4$. The sector corresponded to 1/8 of the discharge chamber and contained five array wires. The simulation region was represented by a numerical mesh consisting of hexahedrons (in the region corresponding to the initial position of the array) and triangular prisms (near the axis). It contained about 5×10^6 of computational cells ($h_\varphi \approx 65$–40 μm, $h_r \approx 60$ μm, and $h_z = 120$ μm). The waveform of the current pulse was specified as $I(t) = I_0 \sin^2\left(\frac{\pi}{2T}t\right)$, the amplitude and rise time of the current pulse being $I_0 = 3$ MA and $T =$ 100 ns, respectively.

The generation of plasma from the wire array material was described in the model of extended plasma production [20]. The rate of plasma mass production was calculated by the formula

$$\dot{m}(t) = \begin{cases} kB^2(t) & \text{for} \quad t < t_\alpha \\ \dfrac{kB^2(t)}{M_0(1-\alpha)}\left(M_0 - m(t)\right) & \text{for} \quad t > t_\alpha, \end{cases} \tag{3}$$

where $k = 0.3$, $\alpha = 0.5$, $B(t)$ is the magnetic field of the discharge current, M_0 is the total array mass, and t_α is determined from the condition $m(t_\alpha) = \alpha M_0$.

Figure 14 presents results of simulations of the implosion of a QTWA with additional mass deposition for the cases of conical and plane electrodes. In the right and left parts of Fig. 14 show results obtained for conical and plane electrodes, respectively. One can see that, in the case of conical electrodes, the central pinch is more compact and the radiation power is two times higher than in the case of plane electrodes.

3D compression of the wire array is achieved due to the profiling of the initial linear mass of the wires. In

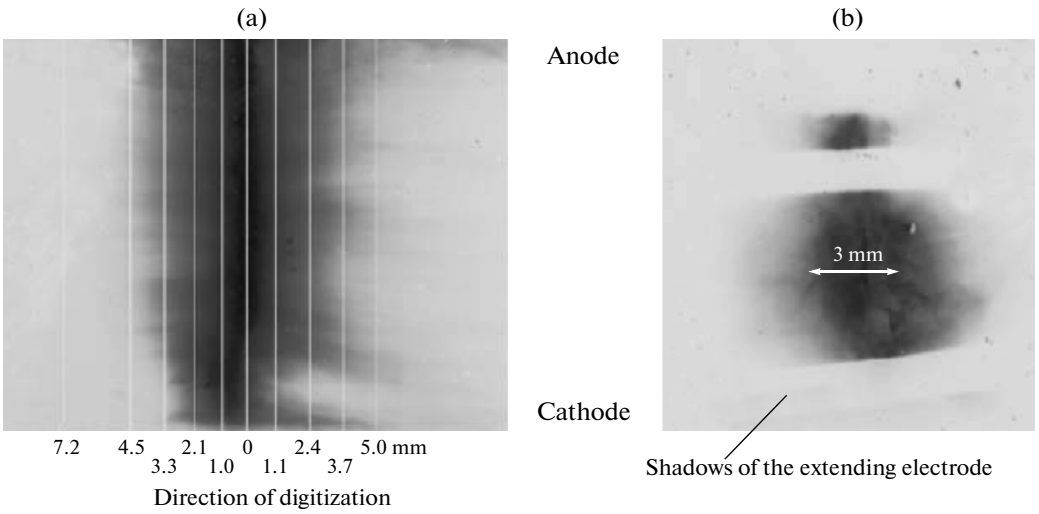

Fig. 12. Time-integrated SXR images of a pinch taken in photons with energies above 120 eV (behind a 316-μg/cm^2 Mylar film) in the implosion of a CTWA and a QMFA with close values of the total array mass: (a) shot no. 5091 (20-mm-diameter cylindrical array made of 40 6-μm-diameter tungsten wires with a total mass of 330 μg) and (b) shot no. 5094 (quasi-spherical array made of 40 25-μm-diameter metalized kapron fibers with a total mass of 270 μg, profiled In–Bi deposition, and conical electrodes). The white vertical lines in panel (a) show the distances from the array axis at which spectra with a radial resolution were obtained using the GIS. The spatial scale in panel (b) is shown by the white double-headed arrow.

this case, the SXR pulse has one peak, whereas without profiling, the emission pulse has two peaks. In the plane-electrode configuration, a fraction of plasma is pushed out toward the cathode and anode and, accordingly, a fraction of kinetic energy leaves the equatorial region. When using truncated conical electrodes, the energy density in the compressed pinch increases substantially. It is seen that, in Fig. 14b, the trailing mass is substantially lower than in Fig. 14a. In addition, in Fig. 14a, escape of plasma from the central region toward the cathode and anode is observed. In the case of truncated conical electrodes (Fig. 14b), plasma does not leave the central region and is compressed toward the array center, which leads to a twofold increase in the X-ray power in Fig. 14d as compared to Fig. 14c.

Thus, the results of numerical simulations of the implosion of QWAs with a profiled linear mass agree well with the experimental data.

The simulations were performed using the following supercomputers: K-100 (Keldysh Institute of Applied Mathematics, Russian Academy of Sciences), MVS-100K (Interdepartmental Supercomputer Center, Russian Academy of Sciences), and Lomonosov (Research Computing Center, Moscow State University).

5. DISCUSSION AND CONCLUSIONS

Analysis of X-ray and optical images recorded in the experiments on QTWA and QMFA implosion carried out at the Angara-5-1 facility at currents of 2–3.5 MA and current rise times of 90–100 ns has shown that the use of arrays with a profiled linear mass and conical electrodes allows one to achieve 3D compression of the array material. The shape of the emission sources observed in the images taken in photons of different hardness is close to spherical. The use of a time-integrated GIS with spatial resolutions along the array radius and height provides a new diagnostic method for studying the pinch compression and the spatial characteristics of pinch radiation in the wavelength range of 20–400 Å for different types of arrays.

Typical radial and axial streak images of an imploding QMFA synchronized with SXR pulses in the photon energy range above 120 eV (shot no. 5094, Fig. 7) allow us to draw important conclusions on spatiotemporal characteristics of the emission source formed during QMFA implosion. The radiation burst in the radial streak image appears at the instant corresponding to the maximum of the SXR power (Fig. 7d), when the plasma from all regions of the array reaches its center. In the axial streak image, radiation from the array center also appears at the instant corresponding to the maximum of the SXR power (Fig. 7e). This means that plasma compression along the radius occurs simultaneously with that along the array height (see the time profiles of the emission intensity in Figs. 7d and 7e), which leads during QMFA implosion. Thus, the single-peak time profile of the SXR pulse indicates synchronous 3D implosion of plasma in the QMFA center.

This conclusion is confirmed by Fig. 8, which shows the waveforms of the discharge current and SXR power and three typical 2D frame X-ray images taken behind different filters at the same instant (4.6 ns before the peak of the SXR power) during QMFA

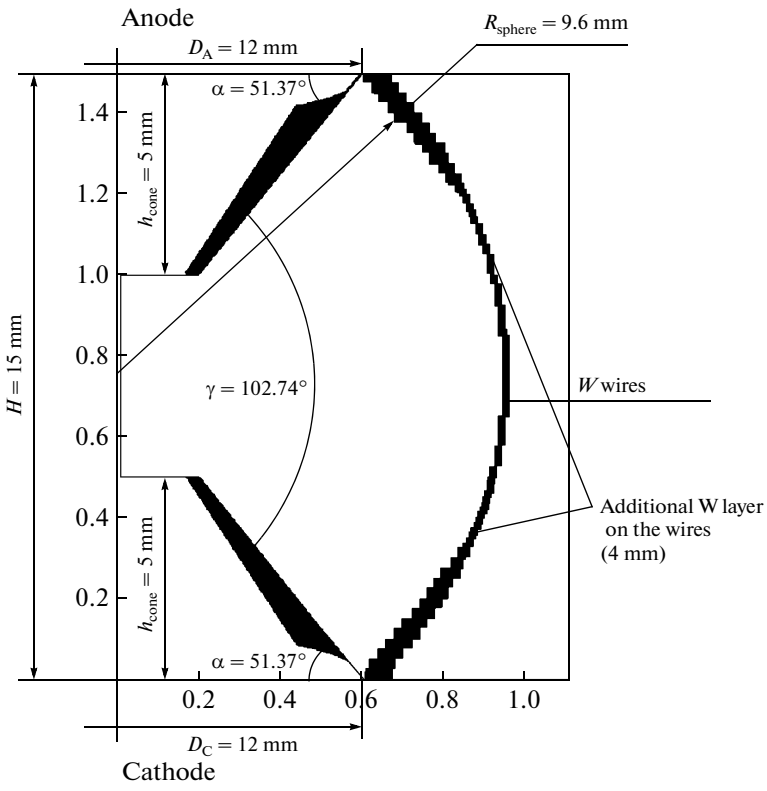

Fig. 13. Scheme of the numerical experiment on studying the implosion of a QTWA with profiled electrodes.

implosion. Indeed, as is seen from the typical frame X-ray image shown in Fig. 8b, the brightest pinch region at the instant corresponding to the maximum of the single-peak SXR pulse is observed in the center of the load.

The SXR spectra recorded with a radial resolution in CTWA implosion (Fig. 11b) show that the radiation spectrum of the trailing mass (curve *3*) differs in character from that of the central part of the pinch (curve *1*), which has typical features of a blackbody source. At the same time, three regions close to the calculated bands in the instantaneous radiation spectra of a tungsten Z-pinch can be distinguished in the radiation spectrum of the trailing mass: 120–250, 80–120, and 45–70 Å [15]. These bands in the spectrum of the trailing mass are related to the reemission of radiation from the central part of the pinch. For the first time, they were observed experimentally in [16]. For a QWAs, in contrast to CWAs, the spectra of the pinch regions spaced from the axis by 2–3 mm remain blackbody in character, but their intensity decreases a factor of 20–30. This indicates a decrease in the trailing mass and the higher compactness of the pinch as compared to those in CWAs.

Thus, it is shown experimentally that the single-peak profile of the SXR pulse and the formation of a quasi-spherical emitting region in the pinch images taken in photons of different hardness indicate the synchronous 3D compression of plasma and 3D concentration of energy in the center of a QMFA with a profiled linear mass and conical electrodes.

In addition to the aforesaid, important indicators of 3D compression of plasma and 3D concentration of energy in the centers of imploding QTWAs and QMFAs are SXR spectra recorded with radial and axial resolutions.

Analysis of spatially resolved SXR spectra (Figs. 9d, 11) shows that, in the course of QTWA implosion, a peak in the range of 100–150 eV appears in the spectrum emitted from the central region of the pinch. The presence of this peak and comparison of these spectra with spatially resolved SXR spectra of an imploding CWA indicates that, due to 3D compression of plasma in the imploding QTWA, the kinetic energy of plasma motion along the array axis makes an additional contribution to the energy of the emission source.

Thus, the results of our experimental studies of the 3D implosion of QWAs, as well as results of computer simulations, allow us to draw the following conclusions.

(i) In the experiments on the implosion of QTWAs and QMFAs with profiled linear masses and conical electrodes carried out at the Angara-5-1 facility at currents of 2–3.5 MA and current rise times of 90–100 ns, 3D compression of the array material has been

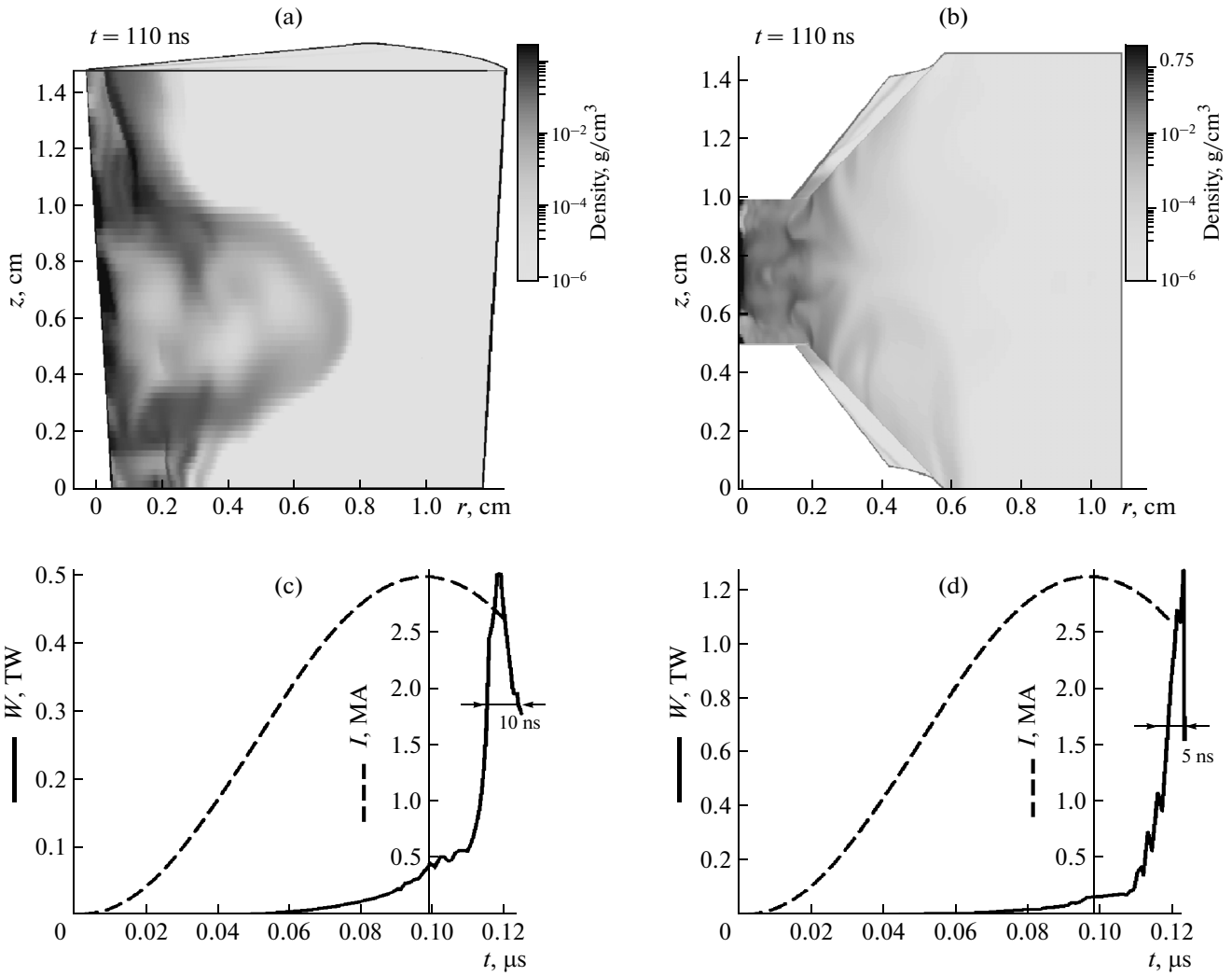

Fig. 14. (a, b) Calculated distributions of the plasma density at the instant of maximum QTWA compression (10 ns after the current maximum) and (c, d) waveforms of the pinch radiation power for mass-profiled arrays with conical (right) and plane (left) electrodes.

achieved and intense quasi-spherical plasma sources of SXR emission have been obtained.

(ii) An increase in the energy density in the center of the SXR emission source formed during the implosion of a QWA with a profiled linear mass has been observed experimentally for the first time. The average energy per unit volume of the emission source formed during QWA implosion is a factor of 7 larger than that formed during the implosion of a CWA with the same mass and a close value of the discharge current in the range of 2.4–3.5 MA.

(iii) The spatial distribution of HXR emission sources in the pinch images taken in photons with energies above 20 keV in the implosion of a QTWA has been studied. It is shown that, in the implosion of such loads, a quasi-spherical HXR source forms in the central region of the array.

(iv) The radial distribution of the SXR intensity in the central region of the emission source and at the array periphery in the implosion of a QTWA has been studied for the first time by analyzing spatially resolved emission spectra in the wavelength range of 20–400 Å.

(v) It is found that, at the initial array diameter of 19 mm, the diameter of the SXR emission source formed during the implosion of a QWA is about 3 mm. The radial compression ratio of plasma in such a source (19 : 3) is higher than that in a CWA (20 : 5) under similar conditions.

(vi) The formation of a peak in the range of 100–150 eV is observed in the emission spectrum recorded with an axial resolution in the implosion of a QTWA with a profiled linear mass. The formation of this peak indicates that the kinetic energy of longitudinal plasma motion during QTWA implosion can additionally contribute to the energy of the radiation source.

(vii) 3D implosion of a QWA with a profiled linear mass and generation of radiation in it have been simulated numerically by using the 3D MARPLE-3D radiative MHD code, developed at the Keldysh Institute of Applied Mathematics, Russian Academy of Sciences. Various configurations of wire arrays have been investigated. The influence of the array geometry and the initial distribution of the array mass on the process of implosion have been studied.

(viii) The numerical simulations have demonstrated that, by appropriately choosing the electrode shape, the array design, and the distribution of the array mass along the wires, it is possible to obtain a bright SXR source in the center of the array. In this case, the SXR pulse has one peak and its power doubles as compared to that in nonoptomized arrays. The results of numerical simulations of the implosion of QWAs with a profiled linear mass agree well with the experimental data.

The further studies in this field will be aimed improving the design and technology of manufacturing of QWAs and QMFAs with the purpose of optimizing 3D concentration of energy in the emission source with allowance for the available data on the plasma production rate [21–25]. To improve the radiative MHD model of the emission source formed during the implosion of QWAs and QMFAs, it is necessary to develop new approaches to calculating the magnetogasdynamic parameters of pinches with allowance for the initial inhomogeneity of plasma production [26, 27] and the influence of magnetic Rayleigh–Taylor instability on the dynamics of implosion and the time profile of SXR emission. To describe the angular anisotropy of the power and spectra of emitted radiation, methods for calculating radiative transfer will be improved by increasing the number of spectral groups and refining the effect of the fine structure of transitions in highly ionized ions, including those in mixtures of elements with medium and high atomic numbers.

ACKNOWLEDGMENTS

We thank the Angara-5-1 team for their engineering and technical support in performing these experiments. This work was supported in part by the Rosatom State Corporation (contract no. H.4X.44.90.13.1108) and the Russian Foundation for Basic Research (project nos. 12-02-00900, 12-02-00369, 13-02-00013, 13-02-00482, and 14-02-00438).

REFERENCES

1. V. P. Smirnov, E. V. Grabovskii, and S. V. Zakharov, JETP Lett. **81**, 442 (2005).
2. D. D. Ryutov, M. S. Derzon, and M. K. Matzen, Rev. Mod. Phys. **72**, 167 (2000).
3. M. G. Haines, Plasma Phys. Controlled Fusion **53**, 093001 (2011).
4. E. V. Grabovskii, A. N. Gritsuk, V. P. Smirnov, V. V. Aleksandrov, G. M. Oleinik, I. N. Frolov, Ya. N. Laukhin, A. N. Gribov, A. A. Samokhin, P. V. Sasorov, K. N. Mitrofanov, and S. F. Medovshchikov, JETP Lett. **89**, 315 (2009).
5. V. V. Aleksandrov, G. S. Volkov, E. V. Grabovski, A. N. Gribov, A. N. Gritsuk, Ya. N. Laukhin, K. N. Mitrofanov, G. M. Oleinik, P. V. Sasorov, and I. N. Frolov, Plasma Phys. Rep. **38**, 315 (2012).
6. E. V. Grabovski, V. V. Aleksandrov, G. M. Volkov, V. A. Gasilov, A. N. Gribov, A. N. Gritsuk, S. V. D'yachenko, V. I. Zaitsev, S. F. Medovshchikov, K. N. Mitrofanov, Ya. N. Laukhin, G. M. Oleinik, O. G. Ol'khovskaya, A. A. Samokhin, P. V. Sasorov, and I. N. Frolov, Plasma Phys. Rep. **34**, 815 (2008).
7. V. V. Aleksandrov, E. V. Grabovski, A. N. Gribov, A. N. Gritsuk, S. F. Medovshchikov, K. N. Mitrofanov, and G. M. Oleinik, Plasma Phys. Rep. **35**, 136 (2009).
8. V. V. Alexandrov, V. E. Fortov, I. N. Frolov, E. V. Grabovskii, I. K. Krasyuk, I. V. Lomonosov, K. N. Mitrofanov, P. P. Pashinin, A. Yu. Semenov, V. P. Smirnov, G. M. Oleinik, I. Yu. Porofeev, V. I. Vovchenko, and G. G. Zukakishvili, in *Proceedings of the 13th International Conference on High-Power Particle Beams, Nagaoka, 2000*, p. 142.
9. V. V. Aleksandrov, E. V. Grabovski, A. N. Gribov, A. N. Gritsuk, S. F. Medovshchikov, G. M. Oleinik, and P. V. Sasorov, Plasma Phys. Rep. **34**, 278 (2008).
10. G. S. Volkov, E. V. Grabovskii, V. I. Zaitsev, G. G. Zukakishvili, M. V. Zurin, K. N. Mitrofanov, S. L. Nedoseev, G. M. Oleinik, I. Yu. Porofeev, V. P. Smirnov, and I. N. Frolov, Instrum. Exp. Tech. **47**, 201 (2004).
11. http://henke.lbl.gov/optical_constants/index.html
12. A. P. Shevel'ko, D. E. Bliss, E. D. Kazakov, M. G. Mazarakis, J. S. McGurn, L. V. Knight, K. W. Struve, I. Yu. Tolstikhina, and T. J. Weeks, Plasma Phys. Rep. **34**, 944 (2008).
13. A. V. Bessarab, S. A. Pospelova, and V. A. Tokarev, Instrum. Exp. Tech. **43**, 573 (2000).
14. K. N. Mitrofanov, E. V. Grabovski, A. N. Gritsuk, Ya. N. Laukhin, V. V. Aleksandrov, G. M. Oleinik, S. F. Medovshchikov, and A. P. Shevel'ko, Plasma Phys. Rep. **39**, 62 (2013).
15. I. Yu. Vichev, V. G. Novikov, and A. D. Solomyannaya, Math. Models Comp. Simulat. **1**, 470 (2009).
16. A. N. Gritsuk, V. V. Aleksandrov, E. V. Grabovskiy, Ya. N. Laukhin, K. N. Mitrofanov, G. M. Oleinik, G. S. Volkov, I. N. Frolov, and A. P. Shevel'ko, IEEE Trans. Plasma Sci. **41**, 3184 (2013).
17. V. A. Gasilov, A. S. Boldarev, S. V. D'yachenko, O. G. Ol'khovskaya, E. L. Kartasheva, S. N. Boldyrev, G. A. Bagdasarov, I. V. Gasilova, M. S. Boyarov, and V. A. Shmyrov, Mat. Model. **24**, 55 (2012).
18. V. Gasilov, A. Boldarev, S. Dyachenko, O. Olkhovskaya, E. Kartasheva, G. Bagdasarov, S. Boldyrev, I. Gasilova, V. Shmyrov, S. Tkachenko, J. Grunenwald, and T. Maillard, in *Advances in Parallel Computing*, Vol. 22: *Applications, Tools and Techniques on the Road to Exascale Computing*, Ed. by K. De Bosschere, E. H. D'Hollander, G. R. Joubert, D. Padua, F. Peters, and M. Sawyer (IOS Press, Amsterdam, 2012), p. 235.

19. A. F. Nikiforov, V. G. Novikov, and V. B. Uvarov, *Quantum-Statistical Models of High-Temperature Plasma and Methods for Calculating Rosseland Mean Free Paths and Equations of State* (Fizmatlit, Moscow, 2000) [in Russian].
20. V. V. Aleksandrov, A. V. Branitsky, G. S. Volkov, E. V. Grabovski, M. V. Zurin, S. L. Nedoseev, G. M. Oleinik, A. A. Samokhin, P. V. Sasorov, V. P. Smirnov, M. V. Fedulov, and I. N. Frolov, Plasma Phys. Rep. **27**, 89 (2001).
21. V. I. Oreshkin, Phys. Plasmas **15**, 092103 (2008).
22. I. I. Beilis, R. B. Baksht, V. I. Oreshkin, A. G. Russkikh, S. A. Chaikovskii, A. Yu. Labetskii, N. A. Ratakhin, and A. V. Shishlov, Phys. Plasmas **15**, 0123501 (2008).
23. V. V. Aleksandrov, E. V. Grabovski, A. N. Gritsuk, Ya. N. Laukhin, S. F. Medovshchikov, K. N. Mitrofanov, G. M. Oleinik, P. V. Sasorov, M. V. Fedulov, and I. N. Frolov, Plasma Phys. Rep. **36**, 482 (2010).
24. K. N. Mitrofanov, E. V. Grabovski, G. M. Oleinik, V. V. Aleksandrov, A. N. Gritsuk, I. N. Frolov, Ya. N. Laukhin, P. V. Sasorov, and A. A. Samokhin, Plasma Phys. Rep. **38**, 797 (2012).
25. V. V. Aleksandrov, K. N. Mitrofanov, A. N. Gritsuk, I. N. Frolov, E. V. Grabovskii, and Ya. N. Laukhin, Plasma Phys. Rep. **39**, 809 (2013).
26. P. Yu. Edmund, M. E. Cuneo, M. P. Desjarlais, R. W. Lemke, D. B. Sinars, T. A. Haill, E. M. Waisman, G. R. Bennett, C. A. Jennings, T. A. Mehlhorn, T. A. Brunner, H. L. Hanshaw, J. L. Porter, W. A. Stygar, and L. I. Rudakov, Phys. Plasmas **15**, 056301 (2008).
27. A. P. Orlov and B. G. Repin, Mat. Model. **26**, 3 (2014).

Translated by A. Nikol'skii